Applied Catalysis A: General 379 (2010) 172–181

Contents lists available at ScienceDirect

Applied Catalysis A: General

journal homepage: www.elsevier.com/locate/apcata

Role of transalkylation reactions in the conversion of anisole over HZSM-5

Xinli Zhu, Richard G. Mallinson, Daniel E. Resasco *

Center for Biomass Refining, School of Chemical, Biological, and Materials Engineering, The University of Oklahoma, 100 East Boyd St., Norman, OK 73019, USA

ARTICLE INFO

Article history:
Received 28 January 2010
Received in revised form 6 March 2010
Accepted 9 March 2010
Available online 15 March 2010

Keywords:
Anisole
Phenolic compounds
HZSM-5
Methoxy group
Biomass conversion
Bio-oil upgrading

ABSTRACT

Conversion of anisole, a typical component of bio-oil, was studied over an HZSM-5 zeolite at varying space times (W/F), reaction temperatures, type of carrier gas, and concentration of water in the feed. Several bimolecular and unimolecular reactions are proposed to explain the evolution of products observed. The bimolecular reactions include the following transalkylation reactions: (a) anisoles to phenol and methylanisole; (b) phenol and methylanisole to cresols; (c) phenol and anisole to cresol and phenol; (d) methylanisole and cresol to phenol and xylenol. A pseudo first-order kinetic model based on these bimolecular reactions was found to describe well the observed product distribution as a function of W/F. It is observed that shape selectivity effects prevail over electrophilic substitution and thermodynamic equilibrium effects in the formation of methylanisole isomers. However, the opposite is true for the distribution of cresol isomers. The kinetic analysis indicates that the contribution of unimolecular reactions such as isomerization is much lower than that of bimolecular reactions. The carrier gas composition was found to have a moderate effect on catalyst activity. When H_2 was used as a carrier, catalyst stability showed a moderate improvement in comparison to the runs under He. However, a remarkable increase in catalytic activity was observed upon the addition of water in the feed.

1. Introduction

Bio-oil derived from lignocellulosic biomass (via fast pyrolysis, high pressure liquefaction, or solvolysis) contains a large variety of oxygenated compounds including acids, aldehydes, ketones, furans, phenolics, sugars, and dehydrosugars, along with large amounts of water [1]. Upgrading this chemically unstable, highly viscous, corrosive, and low-heating value oxygenated mixture to liquid hydrocarbon fuels is an important step in the development of sustainable fuel production [2,3]. Compared to conventional hydrotreating [4–9], bio-oil upgrading via conversion on acid zeolites appears highly attractive as it does not require hydrogen, which increases production costs and may not be readily available in small and distributed plants. Previous studies have demonstrated the effectiveness of zeolites in bio-oil upgrading either during or after pyrolysis [10–18]. However, the highly complex nature of bio-oil requires further studies that can shed light on the possible reaction pathways that each kind of compound and oxygen functionality may undergo in the zeolite.

Phenolic compounds present in bio-oil (phenol, catechol, guaiacol, syringol and their derivatives) arise from the decomposition of lignin fractions in biomass. Depending on the biomass source and the pyrolysis process conditions these compounds can represent a significant fraction of the total bio-oil [2]. Among them, the methoxy phenols (guaiacol, syringol and their derivatives) are particularly abundant. Therefore, it is important to identify the reaction pathways that methoxy phenols may undergo on different zeolites [17–21].

In this contribution, we have focused on the reaction pathways that can occur on acid zeolites when the starting molecule contains the methoxy group ($-OCH_3$). Anisole (or methoxybenzene) is an attractive model molecule to investigate the relative reactivity of the methoxy group, since this is the only functionality in the molecule.

At the same time, anisole is an important primary product from the alkylation of phenol with methanol over acidic catalysts, which further transforms to cresols and xylenols [22–35]. It is generally accepted [26,27,29] that the first step in the conversion of anisole over acid zeolites is the disproportionation to phenol and methylanisole. However, there are some discrepancies on the proposed subsequent transformations to cresols and xylenols; some authors have proposed an intramolecular rearrangement path [29,35] while others support a bimolecular reaction [26,27].

The conversion of anisole over HZSM-5 was systematically studied with varying space time, temperature, feed composition, carrier gas, as well as water addition with the purpose of understanding the reaction pathways and the influence of these variables.

* Corresponding author. Tel.: +1 405 325 4370; fax: +1 405 325 5813.
E-mail address: resasco@ou.edu (D.E. Resasco).

0926-860X/$ – see front matter © 2010 Elsevier B.V. All rights reserved.
doi:10.1016/j.apcata.2010.03.018

2. Experimental

2.1. Catalyst preparation and characterization

NaZSM-5 (supplied by Süd-Chemie, Si/Al = 30) was subjected to three sequential exchanges with NH_4NO_3 at 80 °C. The resultant NH_4ZSM-5 was transformed to H-form by calcination at 550 °C for 4 h.

The powder X-ray diffraction (XRD) pattern of the zeolite was recorded on a Bruker D8 Discover diffractometer, equipped with a Cu Kα radiation source (λ = 1.54056 Å). The morphology of the zeolite was evaluated by high resolution scanning electronic microscopy (SEM) using a Jeol JSM-880 system, equipped with an X-ray elemental analyzer. The acid density was investigated by conventional temperature programmed desorption of adsorbed isopropylamine (IPA-TPD) as detailed elsewhere [36,37].

The coke deposited during reaction was characterized by temperature programmed oxidation (TPO) of 30 mg samples of spent catalyst, under a gas flow of 2% O_2/He (30 mL/min) [37]. The heating ramp was 10 °C/min. The signals of H_2O (m/z = 18), CO_2 (m/z = 44), and CO (m/z = 28) were continuously monitored by a mass spectrometer (MKS). Quantification was achieved by sending calibrated CO_2 and CO pulses (100 μL) into the detector by flowing He. Since both CO and CO_2 are formed during TPO, both contributions to total carbon were considered in the analysis.

2.2. Catalytic measurements

The catalytic performance was evaluated using a quartz tube reactor (0.25 in. o.d.) at atmospheric pressure. In each run (space time of 0.5 h), the catalyst sample (60 mg, 40–60 mesh) was packed in the reactor between two layers of quartz wool. The thermocouple was affixed to the outside wall of the reactor where the catalyst was located. At the start of the experiment, the reactor temperature was increased at 10 °C/min and held at the desired value for 0.5 h in flowing He (20 mL/min) before reaction. When the temperature stabilized, anisole (from Aldrich, 99.7%) was fed by a syringe pump (kd scientific) at a liquid flow rate 0.12 mL/h and vaporized before entering the reactor. All pipelines were heated at 300 °C to avoid condensation of either reactants or products. The products were analyzed online in a gas chromatograph (GC 6890, Agilent), equipped with a flame ionization detector (FID) and a 60 m Innowax capillary column. In parallel, the effluent was trapped in methanol using an ice-water bath, and analyzed by GC–MS (Shimadzu QP2010s) with the same Innowax column, using reference standard compounds for identification. The space time (W/F), expressed in hours, is defined as the ratio between mass of catalyst and the anisole mass flow rate. The conversion and yield (mol.%) were calculated based on the carbon balance.

To monitor the evolution of products as a function of space time over a wide range, both catalyst amount (5–120 mg) and anisole flow rate (0.12–0.36 mL/h, with a He/anisole molar ratio of 50 maintained) were varied. To test the effect of changing the carrier gas, He was replaced by H_2 in several runs, using a H_2/anisole molar ratio of 50. All the gases used in this work were ultra high purity grade, supplied by Airgas Inc. To test the effect of water addition to the feed, deionized water was injected with another syringe pump into the reactant line, keeping a water/anisole mass ratio of 1/4.

3. Results and discussions

3.1. Catalyst characterization

Phase purity of the zeolite was determined by powder X-ray diffraction (XRD). The XRD pattern of the HZSM-5 sample confirmed the MFI structure. SEM was used to assess the crystallite size and shape. Crystallite morphology is important because it determines the diffusion path length of reactants and products inside the zeolite and thus may influence the extent of shape selectivity. SEM observations revealed that the particular HZSM-5 sample used in this study is composed of 1–2 μm aggregates of small primary crystallites that are in the range of 100–200 nm. Elemental analysis confirmed the Si/Al ratio of 30, as reported by the manufacturer. The Brønsted acid density derived from IPA-TPD analysis was 0.523 mmol/g, in good agreement with the theoretical acid density (0.538 mmol/g) that can be calculated from the Si/Al ratio of 30.

3.2. Reaction pathway

3.2.1. Evolution of products with space time (W/F)

To elucidate reaction pathways, the evolution of products with space time was followed at 400 °C. The variation of anisole (An) conversion with W/F is shown in Fig. 1A. The major products and minor product yields are plotted as a function of W/F in Fig. 1B and C, respectively. Major products include methylanisole isomers (MA), phenol (Ph), cresol isomers (Cr), and xylenol isomers (Xol). Minor products include C_{1-9} aliphatic hydrocarbons (mainly C_{1-5}), aromatics (benzene, toluene, xylenes, trimethylbenzene), dimethylanisole isomers (with trace trimethylanisole isomers), trimethylphenol isomers (included in xylenol due to their small amounts and being not well separated), and heavy products (pentamethylbenzenes, naphthalene, methylated naphthalenes), in good accordance with previous work on anisole conversion over HZSM-5 [19,20]. Among the xylenol isomers, the 2,4-xylenol (2,4-Xol) is the dominant isomer, accounting for ~70% of the total isomers; the other five isomers are distributed relatively evenly in small amounts.

As shown in Fig. 1B, at low W/F, phenol and MA exhibit similar yields, while other products remain in small quantities. At higher W/F, phenol continues increasing, while methylanisole passes through a maximum and then gradually drops. At the same time, cresol starts small but its concentration picks up quickly and becomes comparable to that of phenol at high W/F. The xylenol (2,4-Xol) starts with zero derivative and then increases, reaching a plateau. As shown in Fig. 1C, the yields of minor products increase slowly with W/F, starting with zero derivative. All of them appear to be secondary and/or tertiary products.

To determine which of the major products are primary, the yields are plotted in Fig. 2 as a function of anisole conversion, by either varying W/F (full symbols) or temperature (open symbols). It is evident that phenol and MA are primary products initially produced at comparable rates since the slopes at zero conversion are finite and about the same for both. By contrast, cresol and 2,4-xylenol appear as secondary products based on the zero slope observed at anisole conversion approaching zero. The primary products methylanisole and phenol are expected to arise from anisole disproportionation. As the anisole conversion increases, the yields of cresol and 2,4-xylenol increase in a secondary step at the expense of methylanisole.

Based on these results and in agreement with previous studies [26,27,29], the following reactions are proposed (Scheme 1). (1) Two anisole molecules disproportionate to phenol and methylanisole; (2) subsequent reaction of methylanisole with phenol yields two cresol molecules; (3) in turn, cresol and methylanisole can form xylenol and phenol; and (4) phenol reacts with the anisole feed, yielding cresol and another phenol molecule. In addition to these major pathways, several minor pathways take place, including the direct dealkylation of anisole and methylanisole [26,27,29]. The methyl groups eliminated appear as light gases, as observed.

Analysis of the evolution of the isomers of methylanisoles and cresols provides further insight into the reaction pathways. Fig. 1D

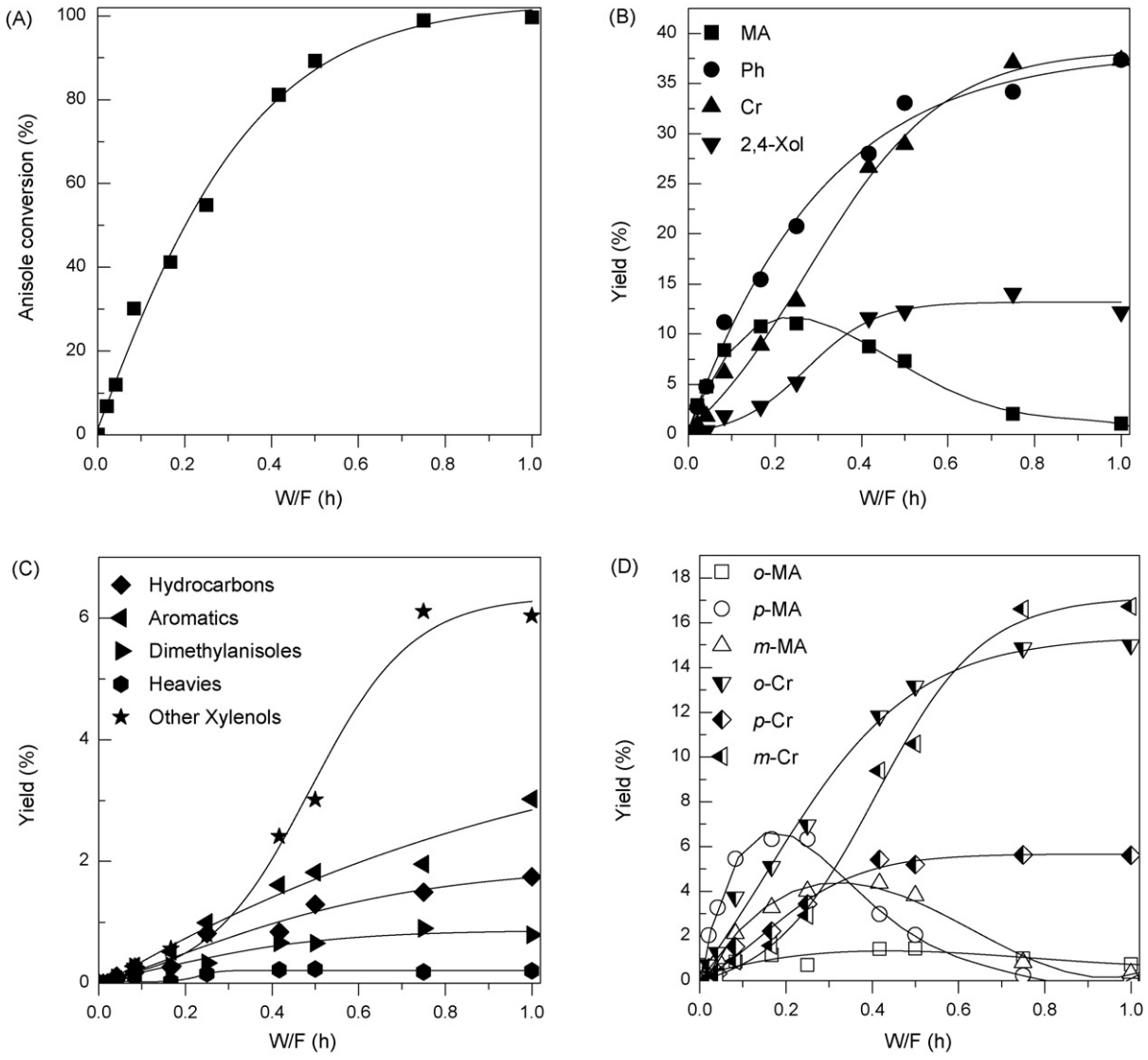

Fig. 1. Effect of space time (W/F) on anisole conversion (A); major product yields (B); minor product yields (C); and methylanisole isomers and cresol isomers distributions (D) over HZSM-5. Reaction conditions: $T = 400\,^{\circ}C$, TOS = 0.5 h.

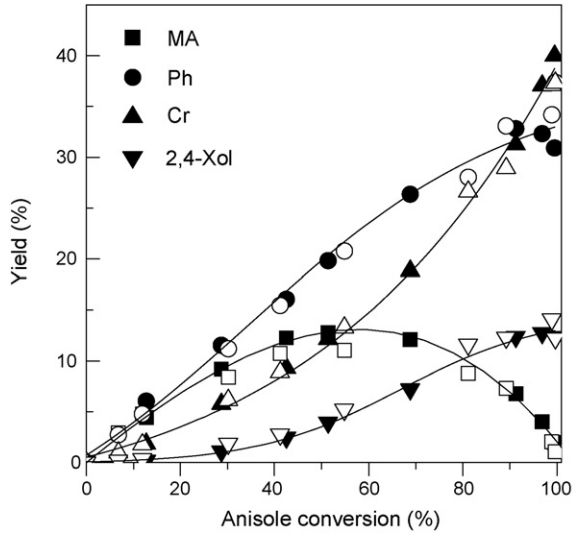

Fig. 2. Effect of anisole conversion on major product yields over HZSM-5. The data were derived from effect of W/F in Fig. 1B (closed symbol) and from effect of reaction temperature in Fig. 5B (open symbol).

shows the evolution of the different isomers as a function of W/F, while Table 1 summarizes the isomer distribution at very low W/F (0.083 h), thus representing the distribution of primary products. It is well known that while the *meta*- (*m*-) position is thermodynamically most favored for substitution in phenol/anisole rings, the *ortho*- (*o*-) position is kinetically favored since it is the most reactive towards electrophilic substitutions [24,31,32]. Also, in the case of zeolite-catalyzed reactions for which shape selectivity may play a role, the *para*- (*p*-) position may be preferentially obtained. As shown in Fig. 1D, it is clear that *p*-methylanisole is the most favorable primary product, but it is also consumed more effectively than other isomers. The evolution of *m*-methylanisole with W/F suggests that after the initial formation, some *p*-methylanisole may isomerize (outside the zeolite channels) to the thermodynamically preferred *m*-methylanisole. Very low yields of *o*-methylanisole are obtained over the entire conversion range. In less confined environments, e.g., amorphous SiO_2–Al_2O_3 or rare earth exchanged Y zeolites the yield of *o*-methylanisole by alkylation of anisole with methanol is comparable or even higher than that of *p*-methylanisole [23]. In this case, our results indicate that shape selectivity is the predominant factor for methylanisole formation, at least in the low conversion range.

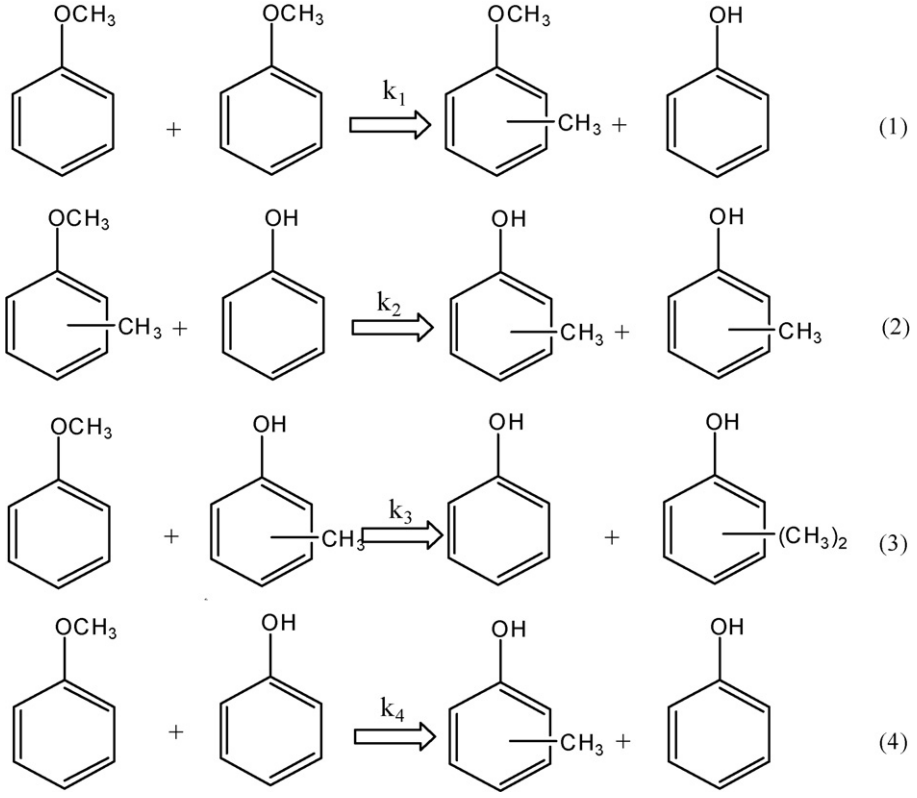

Scheme 1. Proposed major reaction pathways of anisole conversion over HZSM-5 (see Table 2).

The situation is different for the cresol isomers. It is evident that the production of *o*-cresol is dominant at low W/F, indicating that the relatively small size of cresol causes the electrophilic substitution preference to prevail over shape selectivity. The yield of *p*-cresol is higher than that of *m*-cresol at low W/F. At higher W/F, the yield of *m*-cresol increases significantly via isomerization to the thermodynamically most favored isomer [28–31].

The dominant isomer among the xylenols is 2,4-xylenol. This preference could be the result of a combination of shape selectivity and eletrophilic substitution effects since 2,4-xylenol can be formed from anisole reacting with *p*-cresol or *o*-cresol. Xylenols might also be formed from disproportionation of two *o*-cresol molecules; however, this contribution should be much lower than that of the anisole–cresol reaction due to pore size limitation of HZSM-5 since the formation of xylenol may be affected by both transition state shape selectivity and product shape selectivity [38,39].

Table 1
Product distributions (%) for anisole and phenol + anisole conversion over HZSM-5. Reaction conditions: W/F = 0.083 h, anisole or anisole + phenol (1:1), T = 400 °C, TOS = 0.5 h. Kinetic model of 11-reaction model (a); bimolecular reaction model (b); and unimolecular reaction model (c).

Composition (%)	Feed		Model prediction of An + Ph		
	An	An + Ph	a	b	c
Hydrocarbons	0.2	0			
Aromatics	0.2	0.07			
An	73	30	33	31	39
MA	7.7	2.4	1.4	1.6	3
o-MA	0.8	0.1			
p-MA	5	1.6			
m-MA	1.9	0.8			
Dimethyl-An	0.2	0			
Heavies	0	0			
Ph	11	55	53	53	54
Cr	5.7	9.5	11	13	4
o-Cr	3.5	4			
p-Cr	1.4	3.2			
m-Cr	0.8	2.4			
Xol	1.9	2.1	1.3	1.3	0.4
2,4-Xol	1.6	2			
Other Xol	0.26	0.2			

3.2.2. Kinetic model

A simple kinetic model was employed to quantify the contribution of each of the proposed major reaction pathways and determine which paths are dominant. The reaction rate (r_i) for each reaction i is assumed to follow the expression of $r_i = k_i \times C_A \times C_B$, where k_i is the rate constant for reaction i, and C_A and C_B are the concentrations of the reactants A and B. A total 11 elementary reactions are considered, as shown in Table 2, accompanied with the fitted k_i. The fitting of the kinetics data was done using the standard non-linear least square (NLS) routine in Excel Solver.

Table 2
Proposed elementary reactions and fitted reaction rate constant k_i over HZSM-5.

Number	Reaction	Fitted k_i	
		($\times 10^{-5}$ L mol^{-1} h^{-1})	(h^{-1})
1	An + An → Ph + MA	0.032	
2	Ph + MA → Cr + Cr	0.25	
3	Cr + An → Ph + Xol	0.20	
4	Ph + An → Cr + Ph	0.16	
5	MA → Cr		0.093
6	Xol → Cr		0.38
7	Cr → Ph		0.37
8	An → Ph		0.093
9	An → Cr		0.35
10	MA → Xol		0
11	Cr + Cr → Ph + Xol	0	

One of the questions that we had to address in developing the kinetic model was whether the system could be described with unimolecular or bimolecular reactions, or both. For example, Jacobs et al. [29] have suggested that the conversion of anisole on HZSM-5 can be described in terms of a rather simple combination of disproportionation (i.e., 2An → Ph + MA) and unimolecular reactions, i.e., isomerization (An → Cr, MA → Xol) and dealkylation (An → Ph, MA → Cr). However, when we applied this model to the current experimental data, the fit was poor (Fig. S1B). By contrast, when bimolecular reactions were included the fitting improved dramatically (Fig. S1A). Fig. S1A shows the goodness of the fit obtained when bimolecular transalkylation steps were included. The minimum number of steps needed to obtain a good fit was five, four of them bimolecular transalkylations (Scheme 1) and one unimolecular dealkylation (MA → Cr). It is clear that bimolecular reactions are major contributors in the reaction scheme.

After a first approximation using 5 steps, the complete reaction scheme was developed including 11 reaction steps (see Table 2). They are: four bimolecular transalkylation steps (reactions (1)–(4)), four unimolecular dealkylation steps (reactions (5)–(8)), and two unimolecular isomerization steps (reactions (9) and (10)) and cresol disproportionation (reaction (11)). As shown in Fig. 3, an excellent fit of the experimental data is obtained with the proposed set of reaction steps. The robustness of the fitting was tested by varying the set of initial values for the adjustable parameters. In each case, the minimum error was obtained with the same set of final values. The physical implications of the parameters resulting from the fitting can be appreciated by plotting the variation of the rates of the individual reactions as a function of W/F (Fig. 4). First, it can be clearly seen that the reaction rates of the bimolecular reactions (Fig. 4A) are much faster than those of the unimolecular reactions (Fig. 4B). Among the bimolecular reactions, reaction (1) dominates at the reactor inlet, as expected due to the high concentration of anisole. However, soon after, reaction (4) becomes dominant. It is interesting to note that this reaction involves two

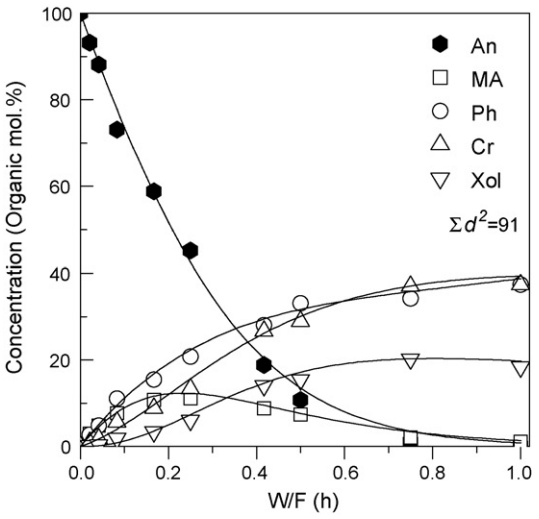

Fig. 3. 11-Reaction kinetic fittings of anisole conversion over HZSM-5. Symbols, experimental data; lines, kinetic fittings. Σd^2 is the total square deviations of fitted data compared to experimental data.

reactants (anisole and phenol) which have significantly smaller kinetic diameters than those of the other molecules, thus we can expect a faster transport rate inside the zeolite channels. Among the unimolecular reactions, the isomerization of An to Cr (reaction (9) in Table 2) and the deakylation of An to Ph (reaction (8)) are more pronounced at low conversion; the deakylation of Xol to Cr (reaction (5)) is noticeable at intermediate conversion and the deakylation of Xol to Cr (reaction (6)) and Cr to Ph (reaction (7)) increase at high conversion.

It must be noted that the bimolecular reactions described in the model do not necessary imply an elementary step. For example, the step indicated as two An molecules yielding a Ph and a Cr molecules

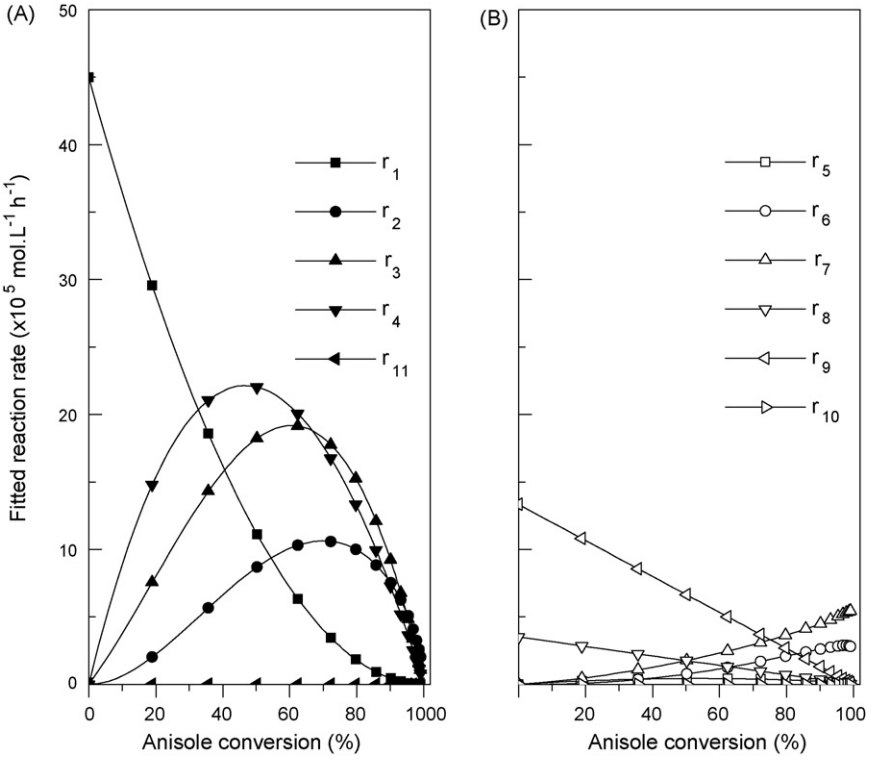

Fig. 4. Comparison of predicted reaction rates of bimolecular (A) and unimolecular (B) reactions over HZSM-5 from the kinetic model and fitted parameters. See reaction numbers in Table 2.

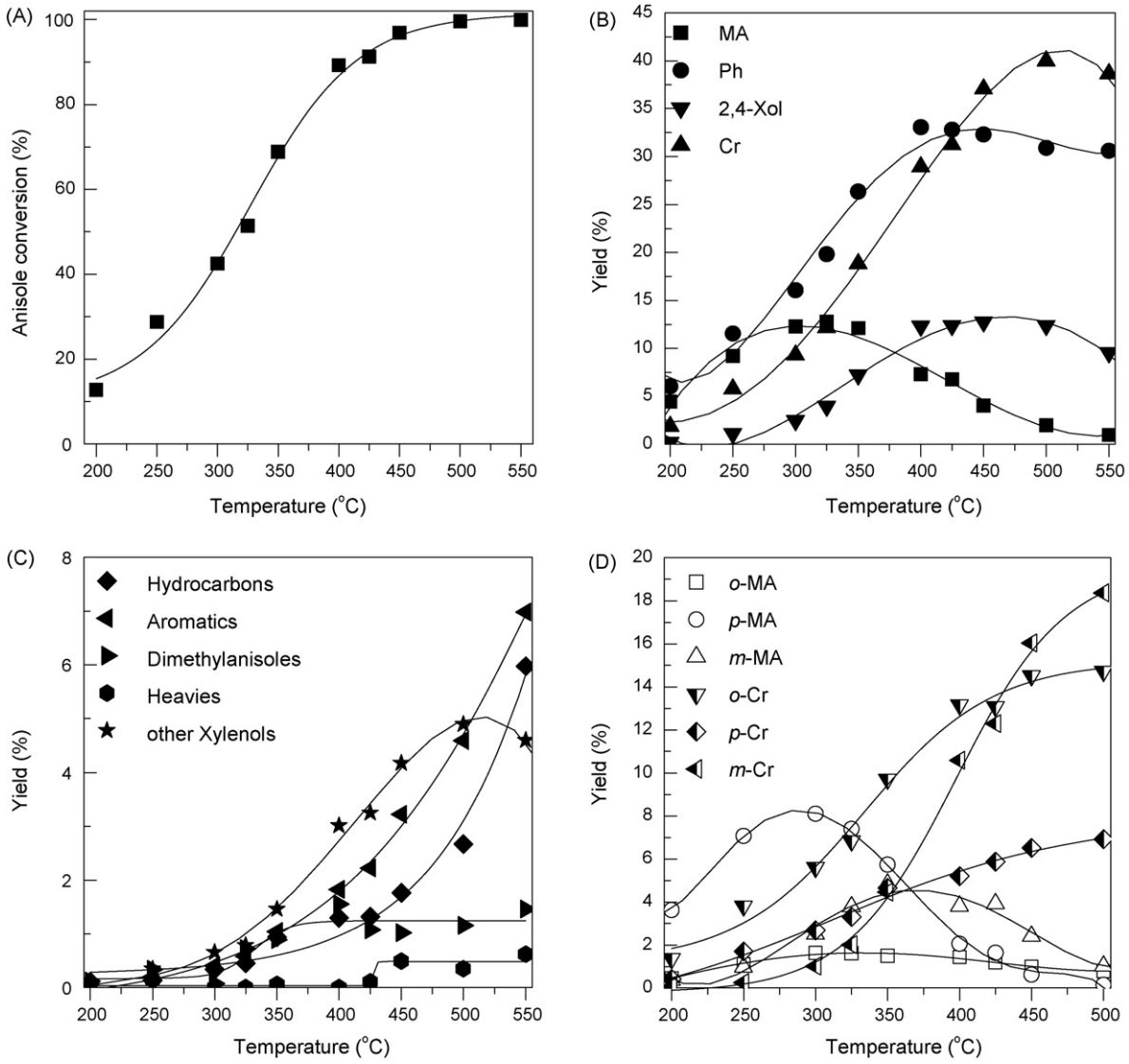

Fig. 5. Effect of reaction temperature on anisole conversion (A); major product yields (B); minor product yields (C); and methylanisole isomers and cresol isomers distributions (D) over HZSM-5. Reaction conditions: W/F = 0.5 h, TOS = 0.5 h.

may in fact occur via an initial decomposition of anisole to Ph and a surface methyl group [40], followed by reaction of this methyl group with another anisole molecule, which yields Cr. However, kinetically this path behaves as if it occurs as 2An to Ph + Cr.

It is well known that xylenes are readily isomerized over HZSM-5. However, it is interesting to note that the isomerization of MA to Xy (reaction (10)) does not seem to occur under the conditions of this study.

3.2.3. Phenol co-feeding

As shown in Scheme 1, since phenol is both a primary product of reaction (1) and a reactant for consecutive reactions (2) and (4), co-feeding phenol with anisole can significantly affect the product distribution. This experiment was tested at a low W/F (0.083 h) to further confirm the proposed reaction pathways for HZSM-5. The results are summarized in Table 1, accompanied by the kinetic model prediction results. It is clear that the addition of phenol to the feed reduces the formation of methylanisole since it competes with the bimolecular transalkylation of anisole (reaction (1)), while it enhances the formation of cresol via reactions (2) and (4), in good agreement with the proposed major reaction pathways. If the reaction followed an intramolecular rearrangement of An to Cr, one would have expected that the addition of phenol would have little effect on the formation of Cr. As shown in Table 1, the 11-reaction model (a) and simplified bimolecular model (b) predict a product distribution from the mixed feed that is closer to that observed experimentally than that predicted by a unimolecular reaction model (c).

3.3. Effect of varying operating conditions

3.3.1. Reaction temperature

The effects of varying reaction temperature were assessed using an intermediate value of W/F in order to obtain a wide range of conversions. Accordingly, the initial conversion as a function of temperature is plotted in Fig. 5 at constant W/F = 0.5 h. It can be seen that in the range 200–500 °C the anisole conversion increases from 14% to 100%. In this range, the yield to methylanisole goes through a maximum at 325 °C. By contrast, phenol, cresol and 2,4-xylenol keep increasing with temperature and only start decreasing above 550 °C, at which temperature thermal cracking becomes significant and causes coke deposition on the reactor walls and quartz wool, in agreement with previous studies of anisole thermolysis in H_2 flow [41]. Yields of dimethyanisoles and heavy compounds increase

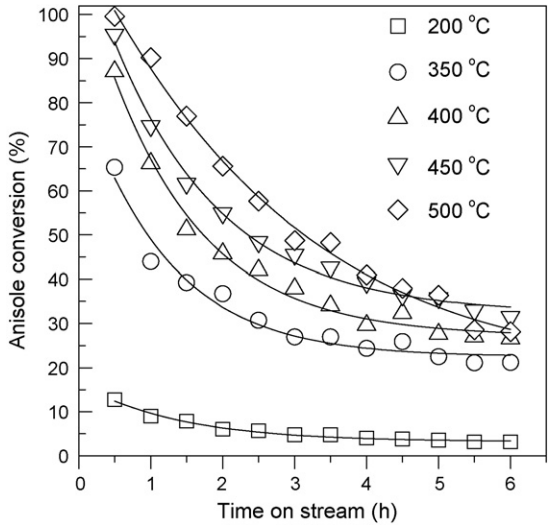

Fig. 6. Anisole conversion as a function of time on stream over HZSM-5 at various temperatures and constant W/F = 0.5 h.

slowly with temperature and remain low over the entire range. By contrast, formation of hydrocarbons and aromatics increases rather quickly with temperature, due to the increase of secondary reactions such as cracking with temperature.

It is interesting to compare the variation of product yield as a function of anisole conversion brought about by either increasing W/F or temperature. As shown in Fig. 2, the major product evolutions fall on the same lines as a function of conversion whether this is varied by increasing temperature (open symbols) or by increasing W/F (full symbols). This is valid up to temperatures close to 550 °C, at which point thermal cracking becomes important.

Another similarity observed in the effect of varying conversion by either increasing temperature or W/F is observed in the distribution of isomers of methylanisole and cresol. The trend shown in Fig. 5D as a function of temperature is similar to that observed in Fig. 1D as a function of W/F. This similarity is expected when the reaction network involves a number of sequential reactions (as those proposed in Scheme 1). If parallel (unimolecular) reactions were more important, one could have expected that differences in activation energies for each step would cause differences in the product evolution as a function of conversion when the temperature is varied compared to the evolution realized by varying W/F at constant temperature.

3.3.2. Time on stream

As shown in Fig. 6, the catalyst deactivates with time on stream at all temperatures. At temperatures below 450 °C, the catalytic activity drops quickly at the beginning of reaction, but then the activity remains rather constant as a function of time. By contrast, at temperatures above 450 °C, the rate of deactivation does not seem to slow down, possibly related to the fast rate of coke formation.

To quantify the amount of coke deposits after reaction, TPO was carried out on spent HZSM-5 as a function of time on stream. Oxidation profiles obtained after several reaction periods at 400 °C at a W/F of 0.5 h are shown in Fig. S2. The shape of the TPO profile does not change with time on stream, while the integrated amounts of C formed after 0.5, 1.0 and 6.0 h on stream are 5.1, 5.6, and 7.3 wt.%, respectively, indicating that most of the carbon is deposited at the beginning of the reaction. Elemental analysis of spent catalyst in anisole conversion [18] showed that the coke contains large amounts of oxygen, suggesting that the sources of coke are probably oxygenates strongly adsorbed on the micropore walls.

Fig. 7A and B shows the CO_2 and H_2O evolution profiles during TPO of the spent catalysts for different reaction temperatures. It can be observed that when the reaction temperature is lower than 450 °C, the CO_2 evolution profile is composed of two overlapping peaks, centered at approximately 545 and 637 °C. With reaction temperature further increased above 450 °C, the two peaks merge into a larger one that shifts to higher oxidation temperatures, up to about 656 °C. At the same time, the evolution profiles of water also shift to higher temperatures, but the intensity does not increase as rapidly as that of CO_2 evolution, indicating that at higher reaction temperatures the coke deposits are leaner in H. The results

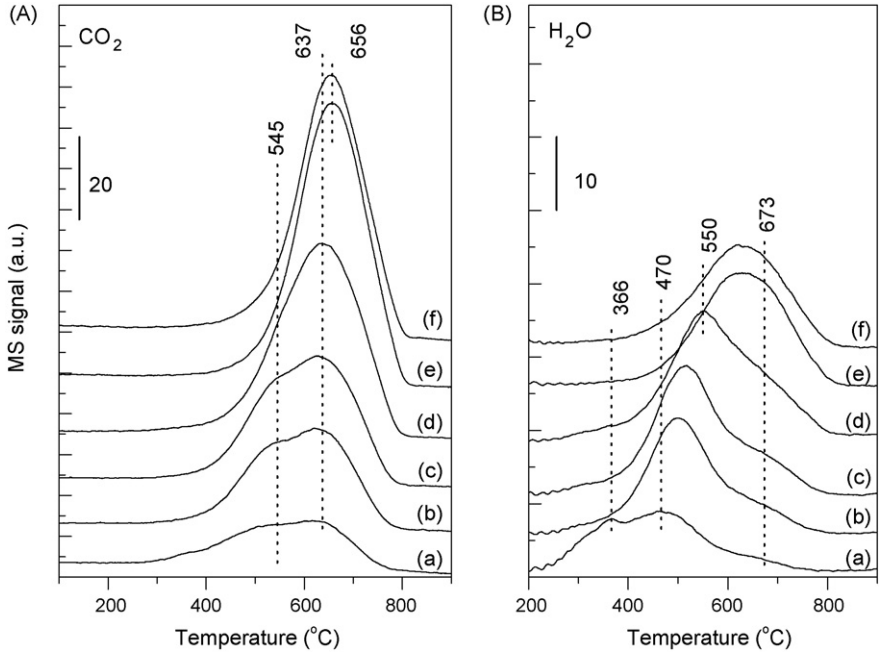

Fig. 7. CO_2 (A) and H_2O (B) evolution profiles during TPO of spent HZSM-5. Reaction condition: (a) 200 °C, (b) 350 °C, (c) 400 °C, (d) 450 °C, (e) 500 °C, (f) 550 °C; W/F = 0.5 h; TOS = 6 h except 550 °C, TOS = 1 h for 550 °C.

Table 3
Amounts of carbon formed on the spent HZSM-5. Reaction conditions: W/F = 0.5 h, TOS = 6 h.

Reaction temperature (°C)	Amount of carbon (wt.%)	A_{CO_2}/A_{H_2O}[a]
200	3.4	1.5
350	6.0	2.1
400	7.3	2.3
450	9.6	2.6
500	12	3.6
550[b]	11	3.4

[a] Integrated intensity ratio between CO_2 signal and H_2O signal of TPO of spent catalyst.
[b] TOS = 1 h.

are quantified in Table 3. It is seen more clearly that the integrated intensity of the CO_2/H_2O ratio increases with reaction temperature, as the coke becomes more refractory.

3.3.3. Carrier gas

As shown in Fig. 8, while the initial anisole conversion using H_2 or He as a carrier gas is the same, the deactivation under H_2 seems to be only slightly slower than under He. TPO of spent catalysts (Fig. S3) showed that the carbon deposition is slightly lower under H_2 (6.65 wt.%) carrier gas than under He (7.26 wt.%). This result indicates that H_2 may play a role in keeping the catalyst surface somewhat cleaner and having a moderate effect in preventing deactivation.

When the catalyst contains a metal function in addition to the acid function, it is well known and easy to understand that the presence of dihydrogen in the gas phase reduces the rate of carbon accumulation [42,43]. However, the effect of hydrogen gas is not as obvious for the case of metal-free zeolites. Nevertheless, it has been reported in several studies that when an inert carrier gas such as He or N_2 is replaced by hydrogen the catalyst stability improves [44–47]. While the experimental fact has been observed clearly, the explanation of this effect has been less unanimous. For example, H_2 activation has been attributed to the presence of metal impurities in the zeolite. Kanai et al. [44] studied metal-free zeolites (Y, Mordenite, ZSM-5) and found them active for ethylene hydrogenation at rather low temperatures (350 °C) and pressures, which they explained in terms of the presence of Fe ions. By contrast, at high temperatures and pressures, conversion of Na ions into Brønsted acid sites has been proposed to occur, which could explain increased activity and stability [45,46]. More directly related to our findings, Meusinger and Corma [46] found that increasing H_2 pressure results in improved stability of HZSM-5 catalysts during n-heptane cracking at 270 °C. They ascribed this phenomenon to a reverse process of hydrocarbon activation over Brønsted acid sites, that is, hydrogen reacts with adsorbed carbenium ions to form carbonium ions, which desorb as paraffins cleaning the surface. In such a process, the Brønsted acid site is regained, leading to a higher stability than under N_2. Henriques et al. have also found that catalyst stability is higher under H_2 than under N_2 during the conversion of *o*-xylene at 350 °C [47]. They found that H_2 inhibits the formation of refractory coke (insoluble in CH_2Cl_2) by changing the balance between hydrogenation and dehydrogenation of coke. These explanations involve the activation of H_2 on acid sites, which is much less effective than on a typical metal catalyst and is more clearly observed at high temperatures and pressures. The role of traces of impurities either on the catalyst or from the gas phase should not be discarded. If hydrogen reacts with traces of oxygenate impurities, it could generate traces of water, which, as shown below may significantly enhance activity.

On the other hand, as shown in Fig. S4, the presence of H_2 does not seem to affect the distribution of products. Both, under He and H_2, the initial major products are phenol, cresol and 2,4-xylenol but their concentration drops with time on stream while methylanisole initially increases and then drops, following the same trend as that seen when varying conversion by changing either temperature or W/F. When plotting the yield of major products as a function of anisole conversion (see Fig. 9) one can see that the yield of all major products fall on the same lines for both carrier gases, suggesting that hydrogen has no effect on the reaction pathway.

3.3.4. Water addition

Since large amounts of water are present in bio-oil [2], the effect of adding water to the anisole feed was investigated. For a standard run with a W/F of 0.5 h, at which the conversion in the absence of water was about 80%, the addition of controlled amounts of water resulted in an increase in activity that led to 100% anisole conversion. Only after for 4 h on stream were slightly lower conversions observed (see Fig. S5). Interestingly, the TPO analysis (Fig. S6) of the spent samples after 6 h on stream showed that the addition of water did not result in less coke, but rather somewhat higher carbon content (8.2 wt.%) than that obtained under

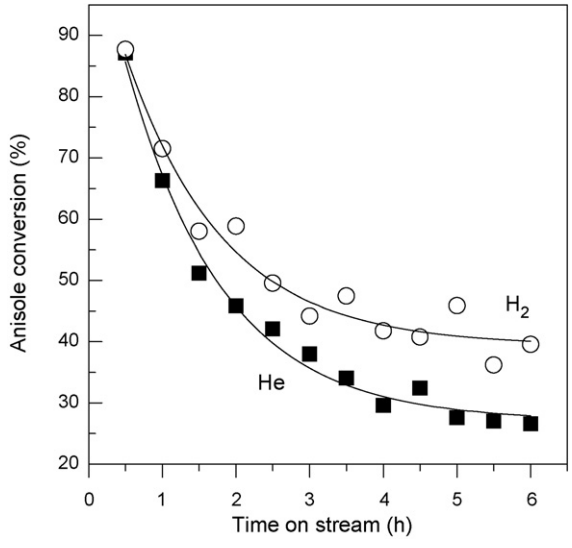

Fig. 8. Effect of carrier gas on anisole conversion over HZSM-5. Reaction conditions: W/F = 0.5 h, T = 400 °C.

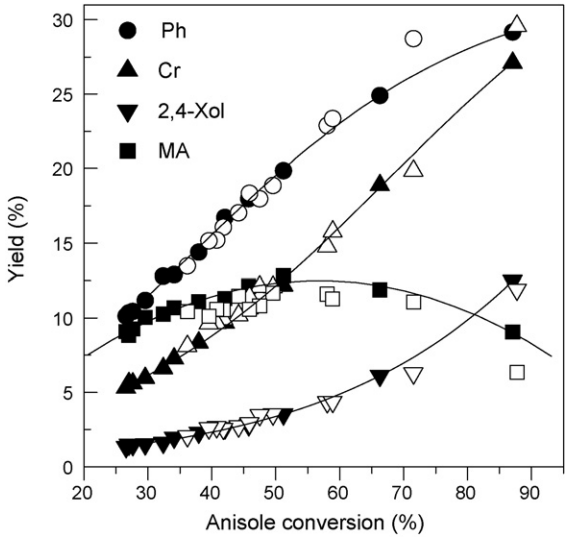

Fig. 9. Effect of carrier gas on major product yields as a function of anisole conversion over HZSM-5. Reaction conditions: W/F = 0.5 h, T = 400 °C. Closed symbol, He carrier; open symbol, H_2 carrier.

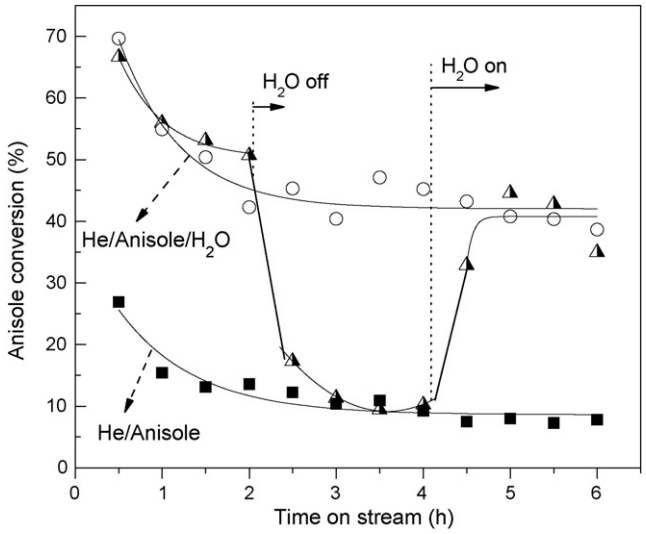

Fig. 10. Effect water addition on anisole conversion over HZSM-5. Reaction conditions: W/F = 0.083 h, 400 °C. Full symbols: no water; open symbols: continuous water addition; half-full symbol: water addition on–off–on.

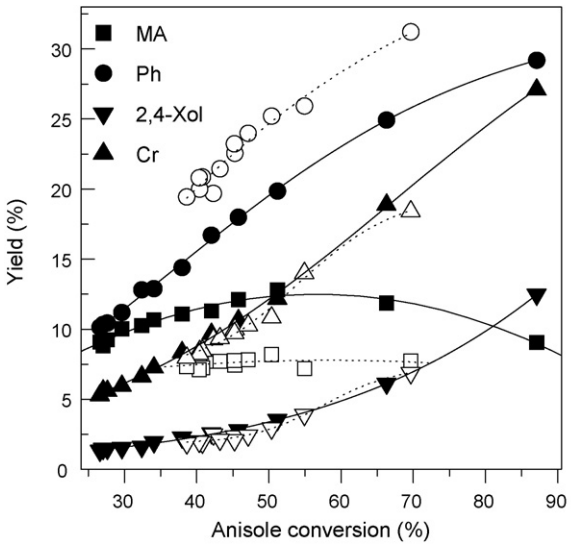

Fig. 11. Effect of water addition on major product yields as a function of anisole conversion over HZSM-5. Reaction conditions: W/F = 0.083 h with water added and W/F = 0.5 h without water condition. The variable conversion data was obtained at varying time on stream. Full symbols: no water; open symbols: with water addition.

similar conditions in the absence of water (7.2 wt.%). As shown in Fig. 10, in order to quantify the effect of water on activity more precisely, additional runs were conducted at lower initial conversions by reducing the W/F to 0.083 h. It can be seen that the initial anisole conversion in the presence of water is ~2.5 times higher than without water. Interestingly, the deactivation rate does not seem to vary with and without water. Therefore, the effect of water cannot be ascribed to a cleaning of coke precursors and a consequent increase in the number of active sites exposed at a given time. Another important result is also included in Fig. 10. It can be seen that when the addition of water was suddenly stopped during the time on stream, the anisole conversion dropped to exactly the same level as that obtained without the addition of water, keeping the same behavior during the 2-h period during which water was not injected. However, the anisole conversion recovered quickly once the water addition was resumed. Moreover, the points lie on the same line as that for which water was kept in the feed for the entire reaction time. These results imply that the positive effect of water is reversible and not associated with the catalyst deactivation. Water is apparently an active species in the reaction process.

To further evaluate the effect of water addition, we plotted in Fig. 11 the yield of major products for the run with water addition as a function of anisole conversion and compared these data with those obtained without the addition of water. In contrast with all the previous comparison of product distribution as a function of conversion, which was the same under different conditions, a clear difference is observed here. While the trends for cresol and 2,4-xylenol yields do not change with water addition, a significant increase in phenol yield at the expense of methylanisole was observed at all conversion levels when water was added. One could ascribe this enhancement to the hydrolysis of the methoxy group in anisole and methylanisole. Since at the entrance of the reactor the anisole concentration is highest, the hydrolysis of anisole not only produces more phenol than without water, but also reduces the contribution of the bimolecular reaction (1), thus decreasing the yield of methylanisole. While the conversion of methylanisole may be increased by hydrolysis, the reduced concentration of methylanisole makes the increase in cresol concentration to be lower. Therefore, the overall effect of water is an increase in anisole conversion and phenol yield with decreased methylanisole yield.

4. Conclusions

Anisole conversion over HZSM-5 has been studied as a model compound in the evaluation of catalysts for bio-oil refining. Anisole contains a methoxy group that provides interesting chemistry. The kinetic analysis indicates that both bimolecular and unimolecular reactions are important in the reaction pathway. At low contact times and higher feed concentrations the reaction is dominated by bimolecular steps involving transalkylation of anisole. Secondary bimolecular reactions involving cresol, phenol and methylanisole become important at higher space time. Several parallel unimolecular reactions also take place. Shape selectivity is evident in the distribution of methylanisole isomers, which are relatively large. By contrast, the distribution of cresol isomers is dominated by electrophilic substitution at low conversions and then by thermodynamic equilibrium.

The same product distribution is obtained with varying conversion by reaction parameters such as reaction temperatures, space time, presence of hydrogen carrier, or catalyst deactivation. By contrast, a significant change in product distribution was observed when water was added to the feed. In addition, the presence of water in the feed was found to improve the activity of the zeolite without altering the stability, probably due to the participation of methoxy group hydrolysis.

Acknowledgements

Financial support from the National Science Foundation EPSCOR (0814361), the Department of Energy (DE-FG36GO88064), and the Oklahoma Bioenergy Center is greatly appreciated.

Appendix A. Supplementary data

Supplementary data associated with this article can be found, in the online version, at doi:10.1016/j.apcata.2010.03.018.

References

[1] D. Mohan, C.U.P. Pittman Jr., P.H. Steele, Energy Fuels 20 (2006) 848–889, and references therein.
[2] G.W. Huber, S. Iborra, A. Corma, Chem. Rev. 106 (2006) 4044–4098, and references therein.

[3] D.E. Resasco, S. Crossley, AIChE J. 55 (2009) 1082–1089.
[4] D.C. Elliott, Energy Fuels 21 (2007) 1792–1815.
[5] E. Furimsky, Appl. Catal. A 199 (2000) 147–190.
[6] C. Zhao, Y. Kou, A.A. Lemonidou, X.B. Li, J.A. Lercher, Angew. Chem. Int. Ed. 48 (2009) 3987–3990.
[7] A. Pinheiro, D. Hudebine, N. Dupassieux, C. Geantet, Energy Fuels 23 (2009) 1007–1014.
[8] T.R. Viljava, E.R.M. Saari, A.O.I. Krause, Appl. Catal. A 209 (2001) 33–43.
[9] C.A. Fisk, T. Morgan, Y.Y. Ji, M. Crocker, C. Crofcheck, S.A. Lewis, Appl. Catal. A 358 (2009) 150–156.
[10] T.R. Carlson, G.A. Tompsett, W.C. Conner, G.W. Huber, Top. Catal. 52 (2009) 241–252.
[11] T.R. Carlson, T.P. Vispute, G.W. Huber, ChemSusChem 1 (2008) 397–400.
[12] M.C. Samolada, A. Papafotica, I.A. Vasalos, Energy Fuels 14 (2000) 1161–1167.
[13] J.D. Adjaye, N.N. Bakhshi, Fuel Process. Technol. 45 (1995) 185–202.
[14] P.T. Williams, P.A. Horne, J. Anal. Appl. Pyrol. 31 (1995) 39–61.
[15] P. Chantal, S. Kaliaguine, J.L. Grandmaison, A. Mahay, Appl. Catal. 10 (1984) 317–332.
[16] A.G. Gayubo, A.T. Aguayo, A. Atutxa, R. Aguado, M. Olazar, J. Bilbao, Ind. Eng. Chem. Res. 43 (2004) 2619–2626.
[17] A.G. Gayubo, A.T. Aguayo, A. Atutxa, R. Aguado, J. Bilbao, Ind. Eng. Chem. Res. 43 (2004) 2610–2618.
[18] J.D. Adjaye, N.N. Bakhshi, Biomass Bioenergy 8 (1995) 131–149.
[19] P.D. Chantal, S. Kaliaguine, J.L. Grandmaison, Appl. Catal. 18 (1985) 133–145.
[20] P.A. Horne, P.T. Williams, Renew. Energy 7 (1996) 131–144.
[21] M.A. Peralta, T. Sooknoi, T. Danuthai, D.E. Resasco, J. Mol. Catal. A 312 (2009) 78–86.
[22] S. Namba, T. Yashima, Y. Itaba, N. Hara, Stud. Surf. Sci. Catal. 5 (1980) 105–111.
[23] L.B. Young, US Patent 4,371,714, (1983).
[24] S. Balsama, P. Beltrame, P.L. Beltrame, P. Carniti, L. Forni, G. Zuretti, Appl. Catal. 13 (1984) 161–170.
[25] R. Renaud, P.D. Chantal, S. Kaliaguine, Can. J. Chem. Eng. 64 (1986) 787–791.
[26] P. Beltrame, P.L. Beltrame, P. Carniti, A. Castelli, L. Forni, Appl. Catal. 29 (1987) 327–334.
[27] M. Marczewski, J.-P. Bodibo, G. Perot, M. Guisnet, J. Mol. Catal. 50 (1989) 211–218.
[28] M. Marczewski, G. Perot, M. Guisnet, Stud. Surf. Sci. Catal. 41 (1988) 273–282.
[29] J.M. Jacobs, R.F. Parton, A.M. Boden, P.A. Jacobs, Stud. Surf. Sci. Catal. 41 (1988) 221–230.
[30] R.F. Parton, J.M. Jacobs, H. Van Ooteghem, P.A. Jacobs, Stud. Surf. Sci. Catal. 46 (1989) 211–221.
[31] N.S. Chang, C.C. Chen, S.J. Chu, P.Y. Chen, T.K. Chuang, Stud. Surf. Sci. Catal. 46 (1989) 223–230.
[32] G. Moon, W. Böhringer, C.T. O'Connor, Catal. Today 97 (2004) 291–295.
[33] M. Bregolato, V. Bolis, C. Busco, P. Ugliengo, S. Bordiga, F. Cavani, N. Ballarini, L. Maselli, S. Passeri, I. Rossetti, L. Forni, J. Catal. 245 (2007) 285–300.
[34] W. Wang, P.L. De Cola, R. Glaeser, I.I. Ivanova, J. Weitkamp, M. Hunger, Catal. Lett. 94 (2004) 119–123.
[35] N. Ballarini, F. Cavani, L. Maselli, A. Montaletti, S. Passeri, D. Scagliarini, C. Flego, C. Perego, J. Catal. 251 (2007) 423–436.
[36] W.E. Fameth, R.J. Gorte, Chem. Rev. 95 (1995) 615–635.
[37] X.L. Zhu, L.L. Lobban, R.G. Mallinson, D.E. Resasco, J. Catal. 271 (2010) 88–98.
[38] F.E. Imbert, S. Gnep, M. Guisnet, J. Catal. 172 (1997) 307–313.
[39] F.E. Imbert, M. Guisnet, S. Gnep, J. Catal. 195 (2000) 279–286.
[40] P. Cheung, A. Bhan, G.J. Sunley, E. Iglesia, Angew. Chem. Int. Ed. 45 (2006) 1617.
[41] I.W.C.E. Arends, R. Louw, P. Mulder, J. Phys. Chem. 97 (1993) 7914–7925.
[42] M. Santikunaporn, J.E. Herrera, S. Jongpatiwut, D.E. Resasco, W.E. Alvarez, E.L. Sughrue, J. Catal. 228 (2004) 100–113.
[43] M.A. Coelho, W.E. Alvarez, E.C. Sikabwe, R.L. White, D.E. Resasco, Catal. Today 28 (1996) 415–429.
[44] J. Kanai, J.A. Martens, P.A. Jacobs, J. Catal. 133 (1992) 527–543.
[45] S. Senger, L. Radom, J. Am. Chem. Soc. 122 (2000) 2613–2620.
[46] J. Meusinger, A. Corma, J. Catal. 152 (1995) 189–197.
[47] C.A. Henriques, A.M. Bentes Jr., P. Magnoux, M. Guisnet, J.L.F. Monteiro, Appl. Catal. A 166 (1998) 301–309.